# MIXED CONVECTION BOUNDARY-LAYER FLOW OF A VISCOELASTIC FLUID DUE TO HORIZONTAL ELLIPTIC CYLINDER WITH CONSTANT HEAT FLUX

by

***Tariq JAVED*** [a*], ***Hussain AHMAD, and Abuzar GHAFFARI*** [b]

[a] Department of Mathematics and Statistics, FBAS, International Islamic University, Islamabad, Pakistan
[b] Department of Mathematics, University of Education, Attock Campus, Pakistan

Original scientific paper
https://doi.org/10.2298/TSCI150120309J

*This article presents numerical analysis of mixed convection laminar flow of a second grade viscoelastic fluid due to cylinder of elliptic cross-section with prescribed surface heat flux. Dimensionless non-linear analysis is computed employing Keller-box method. Skin friction coefficient and Nusselt number are emphasized specifically. These quantities are displayed graphically to examine their behavior along the surface of cylinder. The flow and heat transfer rates are carefully judged while varying the important resulting parameters (mixed convection parameter, viscoelastic parameter aspect ratio, etc.) through sketched graphs keeping major axis of ellipse along and perpendicular to the horizontal. These two positions of major axis are termed as blunt and slender orientations, respectively. The values of skin friction and Nusselt number increase with rise in mixed convection parameter. On the other hand, these quantities lessen by increasing the value of viscoelastic parameter.*

Key words: *mixed convection, viscoelastic boundary-layer flow, elliptic cylinder, aspect ratio, numerical solution*

## Introduction

Convective flows with heat transfer are of much interest to the recent researchers from both theoretical and practical point of view. Such interest stems due to the occurrence of these flows in geophysical and engineering fields including solid matrix heat exchangers, ground water movement, geothermal energy extraction, oil and gas production, thermal insulation drying porous solids, nuclear waste disposals, and many others. Especially mixed convection flows are important in numerous physical situations in environment as well as in artificial appliances, *e. g*. cooling of semi-conductor devices and nuclear power houses, *etc*. For the efficient working of the electronic devices, the cooling through air streams is very easy and economical. To retain working temperature of a system in the industries natural convection and external currents of air are effectively used. The combination of an external source of pushing air and natural convection termed as mixed convection flow. Therefore, the importance of study of mixed convection is recognizable due to its occurrence in nature and in many engineering applications. One of the most important applications of mixed convection flows is cooling of heat exchangers components. Elliptic cylinder shapes are commonly used in the heat exchangers. These cylindrical

* Corresponding author, e-mail: tariq_17pk@yahoo.com

shapes with elliptic cross-section offer smaller resistance to air to pass through and effectively cool the system. Thus, the discovery of efficient and reliable heat exchangers requires a detailed investigation and a careful consideration of heat flows over this kind of geometry. An encyclopedic literature dealing with mixed convection laminar flows over circular cylinder is available but scrutiny of mixed convection flows over the elliptic cylinder needs some serious attention. The pioneering work regarding free convection flows over elliptic cylinder with PST and PHF was carried out by Merkin [1]. Heat-flow was investigated over elliptic cylinder of different eccentricities for both blunt orientation (major axis along horizontal) and slender orientation (major axis along vertical). In another paper, Merkin [2] investigated mixed convection flows over horizontal circular cylinder with PST condition. Bhatacharyya and Pop [3] discussed free convection heat transfer from an elliptical cylinder in flow of micropolar fluids. Hossain *et al.* [4] invented radiation effect over steady natural convection flow over elliptic geometry. Ahmad *et al*. [5] reproduced results of Merkin [1] for constant heat flux case successfully using Keller-box scheme. They presented theoretical results for both air and water to get the concordance with experimental results. Javed *et al*. [6] presented effect of thermal radiation on unsteady mixed convection flow near forward stagnation point over cylinder of elliptic cross-section. They numerically simulated the problem using Keller-box method and calculated the solution at different time steps. Recently, Javed *et al*. [7] discovered mixed convection flow around the elliptic cylinder. In this article, they presented the solution by considering stream velocity as a sine function of eccentric angle. Moreover, a useful contribution in this regards can be seen in the references [8-11].

The study of viscoelastic fluid-flows has also a great importance due to its applications in engineering and several manufacturing processes *e. g*. petroleum drilling, manufacturing of food, paper, paints, coating, inks, and jet fuels, *etc*. The viscoelastic fluid is of second grade nature. Dun and Rajagopal [12] did a comprehensive discussion on second and third order fluids. Ariel [13] and Rajagopal *et al.* [14] also studied viscoelastic fluids in different geometries. It is also necessary here to mention the work done by Cortell [15], Abel *et al.* [16], Hayat *et al*. [17], and Sajid *et al*. [18] on second grade fluids. Recently, Abbas *et al*. [19-21] discussed the hydromagnetic flow of viscoelastic fluid in stretching/shrinking sheet and in semi-porous channel separately. Anwar *et al*. [22] studied the steady mixed convection boundary-layer flow of viscoelastic fluid over a horizontal circular cylinder with constant surface temperature. Later on, Kasim *et al*. [23] investigated the constant heat solution for the viscoelastic boundary-layer flow on circular cylinder. Ahmad *et al*. [24] reported on radiation effect on boundary-layer flow of a viscoelastic fluid over the circular cylinder.

After the persuasion of previously referred work we extended the idea presented in [7] for the second grade viscoelastic fluid model over surface of the cylinder of elliptic cross-section with PHF condition. The drawn numerical outcomes are matched with those presented by Kasim *et al*. [23] for the validation of our solution procedure. This study demonstrated the consequences resulted by varying the emerging parameters on flow and heat transfer rates for both orientations.

## Mathematical analysis

Let us take an elliptic cylinder lying horizontally and consider laminar mixed convection flow of an incompressible, second grade viscoelastic fluid over it. In addition, let lengths of major and minor axis are 2$a$ and 2$b$, respectively. Suppose the fluid be moving with a constant free stream velocity $U_\infty/2$ in the upward direction in such a way that velocity at the edge of boundary-layer is $\overline{u}_e T_\infty$ stands for temperature of ambient fluid and let the surface of cylinder be emitting a constant heat flux $q_w$. The schematic diagram of the problem is given in fig. 1. The

conditions on surface heat flux are $q_w > 0$ and $q_w < 0$ which represent the assisting and opposing flow cases, respectively. The horizontal cylinder is considered enough long to discard end effects. This assumption gives flow field to be 2-D. Along with these assumptions and Boussinesq and boundary-layer approximations, the basic equations [22-24] are:

$$\frac{\partial \overline{u}}{\partial \overline{x}} + \frac{\partial \overline{v}}{\partial \overline{y}} = 0 \tag{1}$$

$$\overline{u}\frac{\partial \overline{u}}{\partial \overline{x}} + \overline{v}\frac{\partial \overline{u}}{\partial \overline{y}} = \overline{u}_e \frac{\partial \overline{u}_e}{\partial \overline{x}} + \nu \frac{\partial^2 \overline{u}}{\partial \overline{y}^2} + \frac{k_0}{\rho}\left(\frac{\partial \overline{u}}{\partial \overline{x}}\frac{\partial^2 \overline{u}}{\partial \overline{y}^2} + \overline{u}\frac{\partial^3 \overline{u}}{\partial \overline{x}\partial \overline{y}^2} + \overline{v}\frac{\partial^3 \overline{u}}{\partial \overline{y}^3} - \frac{\partial \overline{u}}{\partial \overline{y}}\frac{\partial^2 \overline{u}}{\partial \overline{x}\partial \overline{y}}\right) + g\beta(\overline{T} - T_\infty)\sin\phi \tag{2}$$

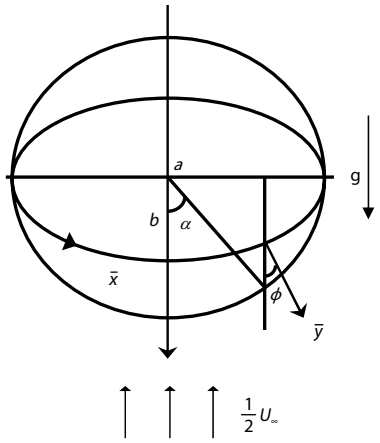


**Figure 1. Schematic diagram of the problem**

$$\rho C_p\left(\overline{u}\frac{\partial \overline{T}}{\partial \overline{x}} + \overline{v}\frac{\partial \overline{T}}{\partial \overline{y}}\right) = k\frac{\partial^2 \overline{u}}{\partial \overline{y}^2} \tag{3}$$

where $\overline{x}$ and $\overline{y}$ are the cartesian co-ordinates, $\overline{u}$ and $\overline{v}$ – the velocity components along $\overline{x}$ and $\overline{y}$, $\overline{T}$ – the temperature, $\nu$ – the kinematic viscosity, $\rho$ – the density, $C_p$ – the specific heat constant, $k$ – the thermal conductivity of the fluid, $k_0$ – the viscoelastic material parameter, g – the gravitational acceleration, $\beta$ – the thermal expansion coefficient, and $\phi$ – the angle measured between downward vertical and outer perpendicular.

In the present study, $k_0$ is taken positive to meet thermodynamic conditions as it was suggested by Dunn and Rajagopal [12]. The Newtonian case can be restored by setting $k_0 + 0$. The related boundary conditions are given by:

$$\begin{aligned} &\overline{u} = 0, \quad \overline{v} = 0, \quad \frac{\partial \overline{T}}{\partial \overline{y}} = -\frac{q_w}{k} \quad at \quad \overline{y} = 0 \\ &\overline{u} \to \overline{u}_e, \quad \overline{T} \to T_\infty \quad as \quad \overline{y} \to \infty \end{aligned} \tag{4}$$

The boundary condition on $\overline{u}$ are two in number but the governing equations representing the problem involve third order derivative of $\overline{u}$ which demands one extra boundary condition. Garg and Rajagopal [25] that extra boundary condition, *i. e.* $\partial \overline{u} / \partial \overline{y} \to 0$ when $\overline{y} \to \infty$, which suffices for the solution of boundary value problem comprising eqs. (1)-(4).

Now introducing the following non-dimensional variables:

$$x = \frac{\overline{x}}{a}, \quad y = \mathrm{Re}^{1/2}\left(\frac{\overline{y}}{a}\right), \quad u = \frac{\overline{u}}{U_\infty}, \quad v = \mathrm{Re}^{1/2}\left(\frac{\overline{v}}{U_\infty}\right), \quad \theta = \frac{\mathrm{Re}^{1/2}\,k}{aq_w}(\overline{T} - T_\infty), \quad u_e = \frac{\overline{u}_e}{U_\infty} \tag{5}$$

into eqs. (1)-(3) we arrive at:

$$\frac{\partial u}{\partial x} + \frac{\partial v}{\partial y} = 0 \tag{6}$$

$$u\frac{\partial u}{\partial x} + v\frac{\partial v}{\partial y} = u_e\frac{\mathrm{d}u_e}{\mathrm{d}x} + \frac{\partial^2 u}{\partial y^2} + K\left(\frac{\partial u}{\partial x}\frac{\partial^2 u}{\partial y^2} + u\frac{\partial^3 u}{\partial x\partial y^2} + v\frac{\partial^3 u}{\partial y^3} - \frac{\partial u}{\partial y}\frac{\partial^2 u}{\partial x\partial y}\right) + \lambda\sin\phi\theta \tag{7}$$

$$u\frac{\partial\theta}{\partial x}+v\frac{\partial\theta}{\partial y}=\frac{1}{\mathrm{Pr}}\frac{\partial^2\theta}{\partial y^2} \tag{8}$$

where are $\mathrm{Re}=aU_\infty/\nu$, $K=k_0U_\infty/a\rho\nu$ is the viscoelastic parameter, $\lambda=\mathrm{Gr}/\mathrm{Re}^{5/2}$ is the mixed convection parameter, and $\mathrm{Pr}=\mu C_p/k$, $\mathrm{Gr}=\mathrm{g}\beta q_w a^4/k\nu^2$.

The mixed convection parameter, $\lambda$, in form of Grashof number gives that with $\lambda>0$ and $\lambda<0$ define assisting flow case and opposing flow case correspondingly. The case $K=0$ restores the Newtonian flow problem.

The boundary conditions (4) along the augmented boundary condition reduces to following form:

$$u=v=0,\quad \frac{\partial\theta}{\partial y}=-1\ \text{ at }\ y=0,\quad u\to u_e,\quad \frac{\partial u}{\partial y}\to 0,\quad \theta\to 0\ \text{ as }\ y=\infty \tag{9}$$

Next we assume the free stream velocity $u_e(\alpha)=\sin\alpha$ where $\alpha$ is the eccentric angle of the ellipse (see fig.1) and introducing the following variables to solve the problem.

$$\psi=xf(x,y),\ \theta=\theta(x,y) \tag{10}$$

with $\psi$ being the usual stream defined by:

$$u=\frac{\partial\psi}{\partial y},\quad v=-\frac{\partial\psi}{\partial x} \tag{11}$$

With these assumptions eq. (6) is identically satisfied and the boundary value problem represented by eqs. (7)-(9) reduces to the following forms:

$$\frac{\partial^3 f}{\partial y^3}+f\frac{\partial^2 f}{\partial y^2}-\left(\frac{\partial f}{\partial y}\right)^2+\frac{\sin\alpha\cos\alpha}{xB}+\lambda\frac{\sin\phi}{x}\theta-K\left[f\frac{\partial^4 f}{\partial y^4}-2\frac{\partial f}{\partial y}\frac{\partial^3 f}{\partial y^3}+\left(\frac{\partial^2 f}{\partial y^2}\right)^2+\right.$$
$$\left.+x\left(\frac{\partial f}{\partial x}\frac{\partial^4 f}{\partial y^4}-\frac{\partial^2 f}{\partial x\partial y}\frac{\partial^3 f}{\partial y^3}+\frac{\partial^2 f}{\partial y^2}\frac{\partial^3 f}{\partial x\partial y^2}-\frac{\partial f}{\partial y}\frac{\partial^4 f}{\partial x\partial y^3}\right)\right]=x\left(\frac{\partial f}{\partial y}\frac{\partial^2 f}{\partial x\partial y}-\frac{\partial f}{\partial x}\frac{\partial^2 f}{\partial y^2}\right) \tag{12}$$

$$\frac{1}{\mathrm{Pr}}\frac{\partial^2\theta}{\partial y^2}+f\frac{\partial\theta}{\partial y}=x\left(\frac{\partial f}{\partial y}\frac{\partial\theta}{\partial x}-\frac{\partial f}{\partial x}\frac{\partial\theta}{\partial y}\right) \tag{13}$$

$$f=\frac{\partial f}{\partial y}=0,\quad \frac{\partial\theta}{\partial y}=-1\ \text{ at }\ \mathrm{y}=0\quad \frac{\partial f}{\partial y}\to\frac{\sin\alpha}{x},\quad \frac{\partial^2 f}{\partial y^2}\to 0,\quad \theta\to 0\ \text{ as }\ y=\infty \tag{14}$$

The geometry shown in fig. 1 clearly demonstrates that when $\sin\phi=\sin x$. The elliptic cylinder reduces to circular cylinder. The study of elliptic cylinder case is confined to two possible cases namely the blunt orientation and slender orientation when major axis of ellipse is considered along horizontal and perpendicular to it, respectively, [1]. The quantities given in eq. (12) $x$, $\sin\phi$, and $B$ are parametrically for blunt as well as slender orientations are:

$$x=\int_0^\alpha\sqrt{1-e^2\sin^2\lambda}\,\mathrm{d}\lambda,\quad \sin\phi=\frac{b\sin\alpha}{a\sqrt{1-e^2\sin^2\alpha}},\quad \text{and } B=\sqrt{1-e^2\sin^2\alpha}$$

and

$$x=\int_0^\alpha\sqrt{1-e^2\cos^2\lambda}\,\mathrm{d}\lambda,\quad \sin\phi=\frac{\sin\alpha}{\sqrt{1-e^2\cos^2\alpha}},\quad \text{and}\quad B=\sqrt{1-e^2\cos^2\alpha}$$

respectively, with $e^2 = 1 - (b^2 - a^2)$ which is square of the eccentricity, $e$, of the ellipse.

The demanding physical quantities skin friction coefficient, $C_f$, and the Nusselt number are defined:

$$C_f = \frac{\tau_w}{\rho U_\infty{}^2} \quad \text{and} \quad \mathrm{Nu} = \frac{aq_w}{k(\overline{T} - T_\infty)} \tag{15}$$

where $\tau_w$ and $q_w$ express the wall shear stress and surface heat flux, respectively, which satisfy:

$$\tau_w = \mu\left(\frac{\partial \overline{u}}{\partial \overline{y}}\right)_{\overline{y}=0} + k_0\left(\overline{u}\frac{\partial^2 \overline{u}}{\partial \overline{x}\partial \overline{y}} + \overline{v}\frac{\partial^2 \overline{u}}{\partial \overline{y}^2} + 2\frac{\partial \overline{u}}{\partial \overline{x}}\frac{\partial \overline{u}}{\partial \overline{y}}\right)_{\overline{y}=0}, \quad q_w = -k\left(\frac{\partial \overline{T}}{\partial \overline{y}}\right)_{\overline{y}=0} \tag{16}$$

Using eqs. (4) and (10), we get:

$$C_f\sqrt{\mathrm{Re}} = x\left(\frac{\partial^2 f}{\partial y^2}\right)_{y=0}, \quad \frac{\mathrm{Nu}}{\sqrt{\mathrm{Re}}} = \frac{1}{\theta(x,0)} \tag{17}$$

The limiting case *i. e.* at the lower stagnation point of the cylinder $x \approx 0$, the PDE (12) and (13) along the boundary conditions to the ODE:

$$f''' + ff'' - (f')^2 + L + \lambda A_0\theta - K\left[ff^{iv} - 2f'f''' + (f'')^2\right] = 0 \tag{18}$$

$$\frac{1}{\mathrm{Pr}}\theta'' + f\theta' = 0 \tag{19}$$

With boundary condition:

$$f(0) = f'(0) = 0, \quad \theta'(0) = -1 \text{ and } \quad f' \to 1, \quad f'' \to 0, \quad \theta \to 0 \text{ as } y = \infty \tag{20}$$

Here the prime notation gives rate of change with respect to $y$ and the quantities $(\sin\alpha\cos\alpha)/xB$ and $\sin\phi/x$ approach to $L$ and $A_0$, respectively, as $x \to 0$. These quantities take the following values $L = 1$, $A_0 = b/a$ for the blunt orientation and $L = A_0 = a^2/b^2$ for the slender orientation.

The eq. (17) reduces to the form:

$$C_f\sqrt{\mathrm{Re}} = xf''(0), \quad \frac{\mathrm{Nu}}{\sqrt{\mathrm{Re}}} = \frac{1}{\theta(0)} \tag{21}$$

## Numerical solution

This section demonstrates the numerical discretization and numerical procedure adopted for the solution of the problem. An implicit finite difference scheme given by Keller and Cebeci [26] is implemented for the solution of governing PDE (12) and (13) with boundary conditions (14). This numerical procedure is very well explained in the book of Cebeci and Bradshaw [27]. The equations are discretized along the whole domain by selecting a suitably small step size in both $x$- and $y$-directions. The grid size $\Delta y = 0.02$ and $\Delta x = \pi / 180$ is found suitable for the present study. The accuracy of achieved results are validated through the benchmark [28] and [23] by setting $\mathrm{Pr} = 1$, $b/a = 1$ (circular cylinder case) and $K = 0$ (Newtonian case). Table 1 shows an excellent concordance of our computed results with the referred results. In this procedure all higher order PDE are reduced to the first order PDE. So, the following variables are introduced:

$$f_y = u, \quad f_{yy} = v, \quad f_{yyy} = w, \quad f_{yyyy} = g, \quad \text{and} \quad \theta_y = q$$

then the governing eqs. (12)-(14) reduces to:

$$v' + fv - u^2 + \frac{\sin\alpha\cos\alpha}{x.B} + \lambda\frac{\sin\phi}{x}\theta - K\left[fg - 2uw + v^2 + \right.$$
$$\left. + x\left(ug - w\frac{\partial u}{\partial x} + v\frac{\partial v}{\partial x} - u\frac{\partial w}{\partial x}\right)\right] - x\left(u\frac{\partial u}{\partial x} - v\frac{\partial f}{\partial x}\right) = 0$$
$$\frac{1}{\mathrm{Pr}}q' + fq - x\left(u\frac{\partial\theta}{\partial x} - q\frac{\partial f}{\partial x}\right) = 0$$
$$f(x,0) = u(x,0) = 0, \quad q(x,0) = -1$$
$$u(x,\infty) = \frac{\sin\alpha}{x}, \quad v(x,\infty) = 0, \quad \theta(x,\infty) = 0$$

The uniform grid points are taken in ($x$, $y$) plane which are defined:

$$x^0 = 0, \quad x^n = x^{n-1} + k, \quad y_0 = 0, \quad y_j = y_{j-1} + h$$

where:

$$j = 1,2,.....M \quad \text{and} \quad n = 1,2,.....N$$

with $n$ and $j$ being positive integers showing the grid location in the ($x$, $y$). The derivatives with respect to $x$ and $y$ are discretized by the formulas given below:

$$(\,)_j^{n-\frac{1}{2}} = \frac{1}{k}\left[(\,)_j^n - (\,)_j^{n-1}\right] \quad \text{and} \quad (\,)_{j-\frac{1}{2}}^n = \frac{1}{h}\left[(\,)_j^n - (\,)_{j-1}^n\right]$$

and the function's value is taken as average value at two consecutive grid points:

$$(\,)_j^{n-\frac{1}{2}} = \frac{1}{2}\left[(\,)_j^n + (\,)_j^{n-1}\right] \quad \text{and} \quad (\,)_{j-\frac{1}{2}}^n = \frac{1}{2}\left[(\,)_j^n + (\,)_{j-1}^n\right]$$

The Newton's linearization is employed to linearize highly non-linear PDE in the following fashion:

$$\left(f_j^n\right)^{i+1} = \left(f_j^n\right)^i + \left(\delta f_j^n\right)^i, \quad \left(u_j^n\right)^{i+1} = \left(u_j^n\right)^i + \left(\delta u_j^n\right)^i$$
$$\left(v_j^n\right)^{i+1} = \left(v_j^n\right)^i + \left(\delta v_j^n\right)^i, \quad \left(w_j^n\right)^{i+1} = \left(w_j^n\right)^i + \left(\delta w_j^n\right)^i$$
$$\left(g_j^n\right)^{i+1} = \left(g_j^n\right)^i + \left(\delta g_j^n\right)^i, \quad \left(\theta_j^n\right)^{i+1} = \left(\theta_j^n\right)^i + \left(\delta\theta_j^n\right)^i$$
$$\left(q_j^n\right)^{i+1} = \left(q_j^n\right)^i + \left(\delta q_j^n\right)^i$$

By supplying a suitable initial guess, we obtain a linear system of algebraic equations, which is solved using tri-diagonal elimination to get the solution at next grid point.

## Results and discussion

The non-dimensional PDE (12) and (13) with boundary conditions (14), and ODE (18) and (19) with boundary conditions (20) are integrated numerically using an implicit finite difference scheme, *i. e.* Keller-box method. The details of the scheme are given in [26, 27]. The grid size along $y$-direction $\Delta y$ and $y_\infty$ is carefully varied adjusted for various choices of pertinent parameters to get highly accurate results. Therefore, the grid size $\Delta y$ = 0.02 and $\Delta x = \pi/180$ has found suitable for present numerical study. The calculations of results are start-

**Table 1. The values of $f''(0)$ and $\theta(0)$ for various values of $\lambda$ with Pr = 1, $b/a = 1$, and $K = 0$ (Newtonian fluid)**

| $\lambda$ | $f''(0)$ | | | $\theta(0)$ | | |
|---|---|---|---|---|---|---|
| | [28] | [23] | Present | [28] | [23] | Present |
| –0.7 | – | 0.247743 | 0.24794 | – | 2.220434 | 2.2201 |
| –0.6 | 0.4925 | 0.490622 | 0.49056 | 2.0547 | 2.057117 | 2.0572 |
| –0.4 | 0.7998 | 0.798697 | 0.79866 | 1.9046 | 1.906045 | 1.9061 |
| –0.2 | 1.0340 | 1.033028 | 1.033 | 1.8157 | 1.816890 | 1.8169 |
| 0 | 1.2336 | 1.232658 | 1.2326 | 1.7517 | 1.752872 | 1.7529 |
| 0.2 | 1.4117 | 1.410764 | 1.4107 | 1.7018 | 1.702823 | 1.7029 |
| 0.4 | 1.5747 | 1.573759 | 1.5737 | 1.6608 | 1.661736 | 1.6618 |
| 0.6 | 1.7263 | 1.725350 | 1.7253 | 1.6260 | 1.626904 | 1.6269 |
| 0.8 | 1.8690 | 1.867919 | 1.8679 | 1.5958 | 1.596697 | 1.5967 |
| 1.0 | 2.0042 | 2.003106 | 2.0031 | 1.5692 | 1.570047 | 1.5701 |
| 1.4 | 2.2570 | 1.255786 | 2.2557 | 1.5239 | 1.524693 | 1.5247 |
| 1.8 | 2.4913 | 2.489892 | 2.4898 | 1.4863 | 1.487048 | 1.4871 |
| 3.0 | 3.1171 | 3.115282 | 3.1152 | 1.4015 | 1.402232 | 1.4022 |
| 4.0 | 3.5784 | 3.576073 | 3.576 | 1.3500 | 1.350735 | 1.3507 |
| 5.0 | 4.0019 | 3.999106 | 3.999 | 1.3088 | 1.309546 | 1.3096 |
| 6.0 | 4.3967 | 4.393430 | 4.3933 | 1.2746 | 1.275348 | 1.2754 |
| 7.0 | 4.7686 | 4.764909 | 4.7647 | 1.2455 | 1.246194 | 1.2462 |
| 8.0 | 5.1217 | 5.117609 | 5.1174 | 1.2201 | 1.220844 | 1.2209 |
| 9.0 | 5.4591 | 5.454494 | 5.4543 | 1.1977 | 1.198462 | 1.1985 |
| 10.0 | 5.7730 | 5.777805 | 5.7776 | 1.1770 | 1.178456 | 1.1785 |

ed at lower stagnation point and continue the process along the surface of cylinder to the point where solution exists and separation does not occur. To assure the accuracy of computed results, we have matched them to those earlier reported by Kasim *et al*. [23] and Nazar *et al.* [28] setting Pr = 1, $b/a = 1$ (circular cylinder case), and $K = 0$ (Newtonian case). Table 1 shows an excellent concordance of our computed results with referred results.

The profiles of key physical quantities – the skin friction $C_f \mathrm{Re}^{1/2}$ and Nusselt number $\mathrm{NuRe}^{-1/2}$ for blunt orientation case are displayed in figs. (2)-(5). Figures 2(a) and 2(b) illustrate the $C_f \mathrm{Re}^{1/2}$ and $\mathrm{NuRe}^{-1/2}$ for various options while other parameters are kept fixed. It is noted that by the enhancement of the value of mixed convection parameter both flow and heat transfer rates boost. Also due to this increase in mixed convection, boundary-layer separation delays. It is further seen that the flow rate achieves its maximum value along the surface of cylinder before separation initiates.

Figures 3(a) and 3(b) indicate the behavior of $C_f \mathrm{Re}^{1/2}$ and $\mathrm{NuRe}^{-1/2}$ along the surface of cylinder for various choices of aspect ratio $b/a$ both in the cooled cylinder case ($\lambda = -0.3$) and heated cylinder case ($\lambda = 2$). The solid curves give the trend of these quantities in cooled cylinder case and dotted curves express them in heated cylinder case. It is observed that by extending aspect ratio $b/a$, both flow and heat transfer rates decrease in the cooled cylinder case and boundary-layer separation comes early. On the oth-

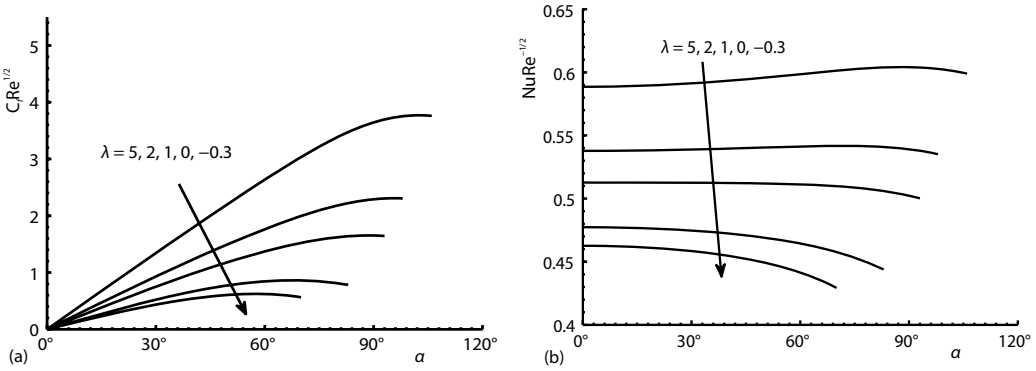


**Figure 2. (a) The change in $C_f Re^{1/2}$ and (b) $NuRe^{-1/2}$ for various values mixed convection parameter $\lambda$ when $K = 0.2$, $b/a = 0.5$, and Pr = 0.7**

er hand, the same quantities show the reverse trend by extending the aspect ratio. A slight rise in the flow rate is noted by increasing the aspect ratio $b/a$. The heat transfer rate grows along the surface of cylinder in the interval $0 < \alpha < 42^o$ but declines in the interval $69^o < \alpha < 86^o$ by extending the aspect ratio of the elliptic cylinder. The change of behavior of heat transfer rate is shown in the interval $42^o < \alpha < 69^o$ by extending the aspect ratio.

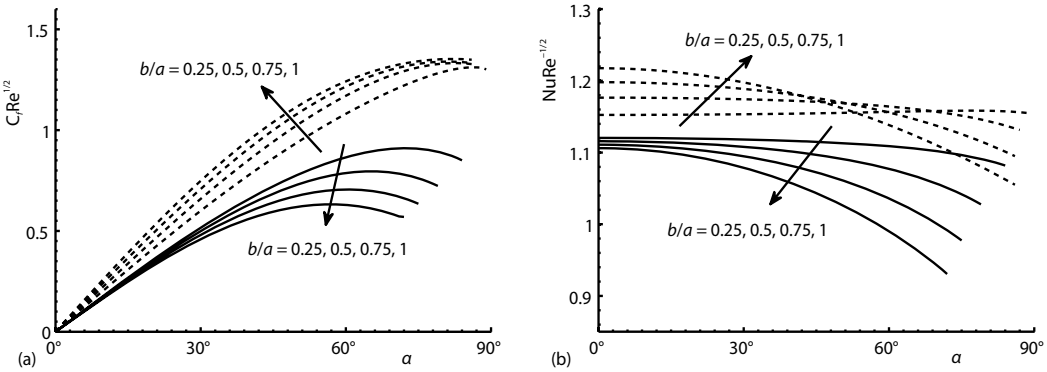


**Figure 3. (a) The change in $C_f Re^{1/2}$ and (b) $NuRe^{-1/2}$ for separate values of aspect ratio $b/a$ when $K = 0.2$, $\lambda = -3$ (solid curves), $\lambda = 2$ (dotted curves), and Pr = 7**

Figures 4(a) and 4(b) express the trend of flow and heat transfer rates along the surface of cylinder for various options of viscoelastic parameter, $K$, while keeping the other parameters fixed. Both flow and heat transfer rates obviously decrease by the growth of viscoelastic parameter that agrees with the practical situations. Figures 5(a) and 5(b) show the impact of Prandtl number on flow and heat transfer rates along the surface of cylinder. Both quantities decrease due to rise in the value of Prandtl number, but the boundary-layer separation delays by lessening the value of Prandtl number.

The flow and heat transfer rates in case of slender orientation are displayed in figs. 6-10. The rise in flow and heat transfer rates due to growth of mixed convection parameter, $\lambda$, along the surface of cylinder. The phenomenon is displayed in figs. 6(a) and 6(b). It is interestingly noted that by raising the mixed convection parameter to a specific value $\lambda_c$ the boundary-layer separation delays. But the separation initiates early for $\lambda > \lambda_c$. The increase in flow and heat transfer rates due to the extension of aspect ratio for the range $0 < b/a < 0.5$ but decrease

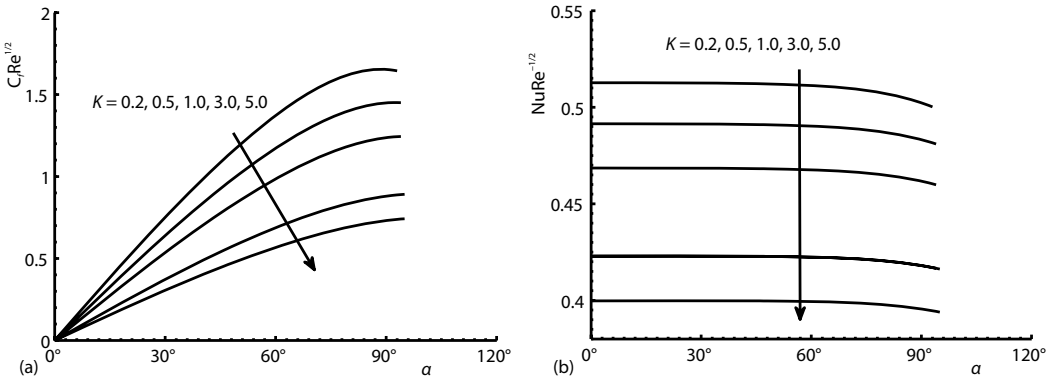


**Figure 4. (a) The change in $C_f Re^{1/2}$ and (b) $NuRe^{-1/2}$ for various values of viscoelastic parameter, $K$, when $\lambda = 1$, $b/a = 0.5$, and Pr = 1**

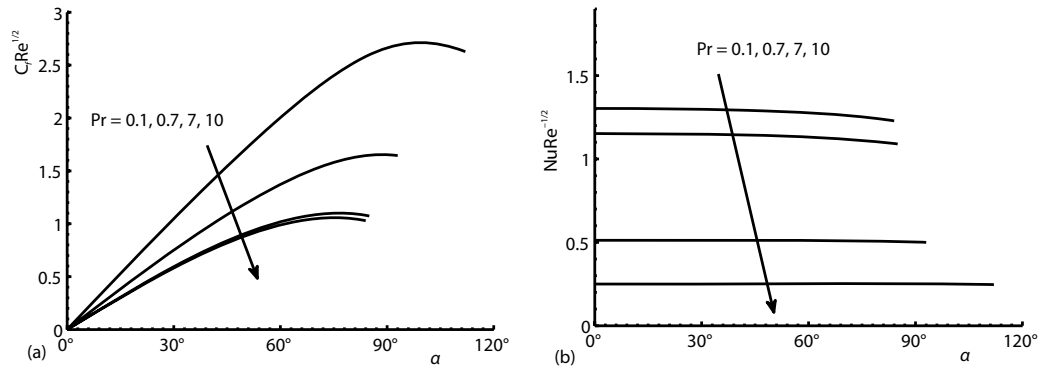


**Figure 5. The change in (a) $C_f Re^{1/2}$ and (b) $NuRe^{-1/2}$ for various values of Prandtl number when $\lambda = 1$, $b/a = 0.5$, and $K = 0.2$**

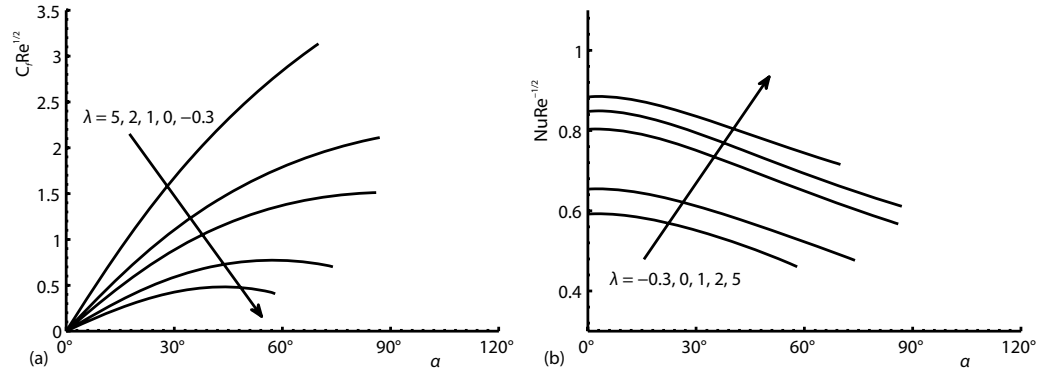


**Figure 6. (a) The variation of $C_f Re^{1/2}$ and (b) $NuRe^{-1/2}$ for different values of mixed convection parameter when $K = 0.2$, $b/a = 0.5$, and Pr = 07**

in the value of both quantities for $b/a$ in the range $0.5 < b/a < 1$ is noticed in the cooled cylinder case. This fact is shown in figs. 7(a) and 7(b). Figures 8(a) and 8(b) illustrate the trend of flow and heat transfer rates for the different choices of the aspect ratio in case of heated cylinder. It is noticed that the flow rate increases but heat transfer rate decreases by extending the aspect ratio. The boundary-layer separation delays on the other hand. Figures 9(a) and 9(b) indicate

the effect of viscoelastic parameter on flow and heat transfer rates. Obviously, both quantities decrease due to the growth in value of viscoelasticity of the fluid as in case of blunt orientation.

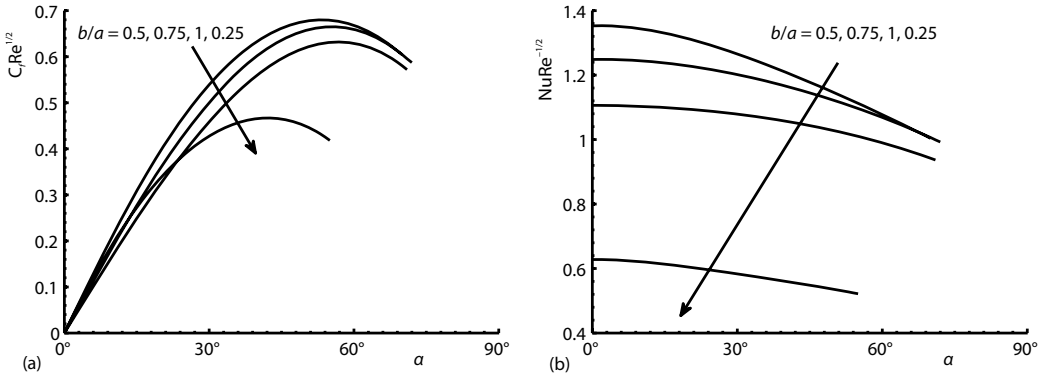


**Figure 7. (a) The variation of $C_f\,\mathrm{Re}^{1/2}$ and (b) $\mathrm{NuRe}^{-1/2}$ for different values of aspect ratio $b/a$ when $K = 0.2$, $\lambda = 0.3$, and Pr = 7**

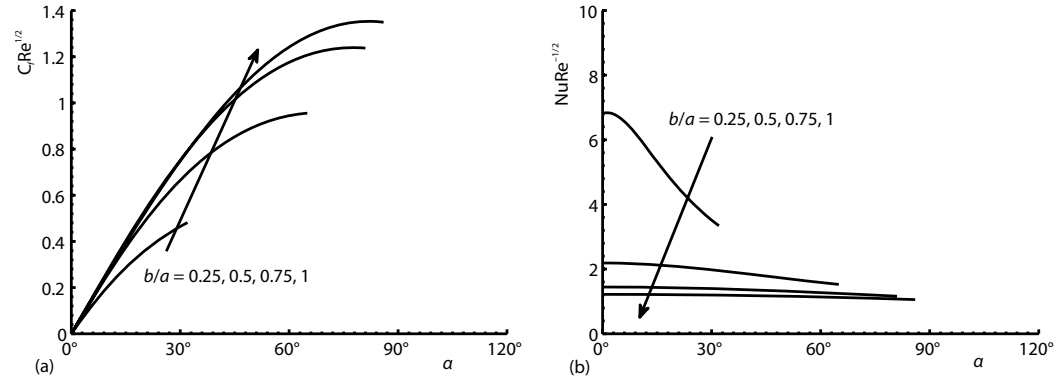


**Figure 8. (a) The variation of $C_f\,\mathrm{Re}^{1/2}$ and (b) $\mathrm{NuRe}^{-1/2}$ for the various values of parameter $b/a$ with $K = 0.2$, $\lambda = 2$, and Pr = 7**

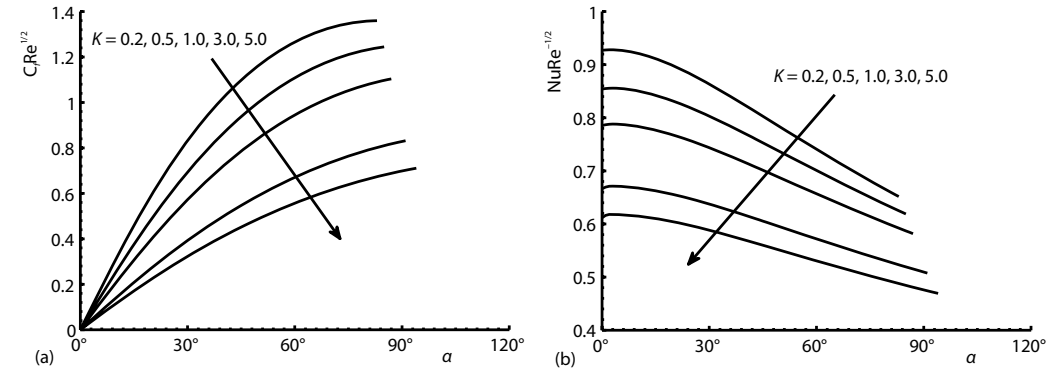


**Figure 9. (a)The variation of $C_f\,\mathrm{Re}^{1/2}$ and (b) $\mathrm{NuRe}^{-1/2}$ for various values of viscoelastic parameter, $K$, when $\lambda = 1$, $b/a = 0.5$, and Pr = 1**

Figures 10(a) and 10(b) display the trends of both flow and heat transfer rates for various values of the Prandtl number. It is noticed that both quantities decline with the rise in value of Prandtl number. Figures 11(a) and 11(b) show the velocity and temperature profile in the boundary-layer for various options of viscoelastic parameter, $K$, at the eccentric angle $\alpha = 30^{o}$ in the blunt orientation case. The velocity reduces due to the increase in viscoelasticity of the fluid on the other hand temperature increases in the boundary-layer.

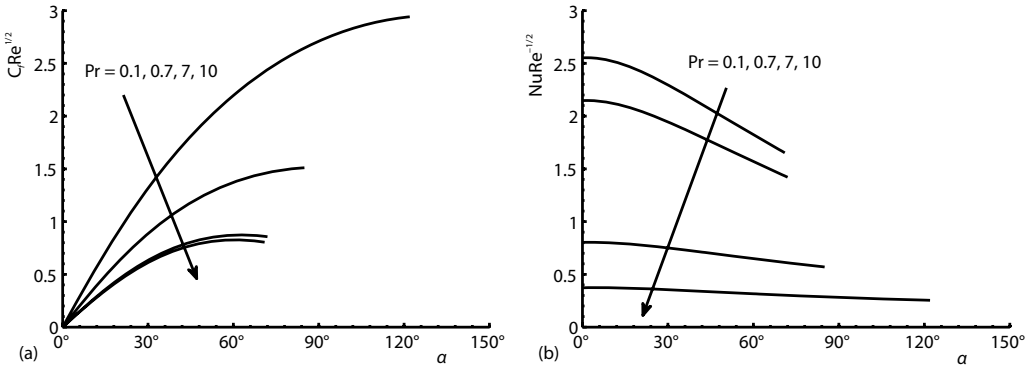


**Figure 10. (a) The change in $C_f\,\mathrm{Re}^{1/2}$ and (b) $\mathrm{NuRe}^{-1/2}$ for various values of Prandtl number Pr when $\lambda = 1$, $b/a = 0.5$, and $K = 0.2$**

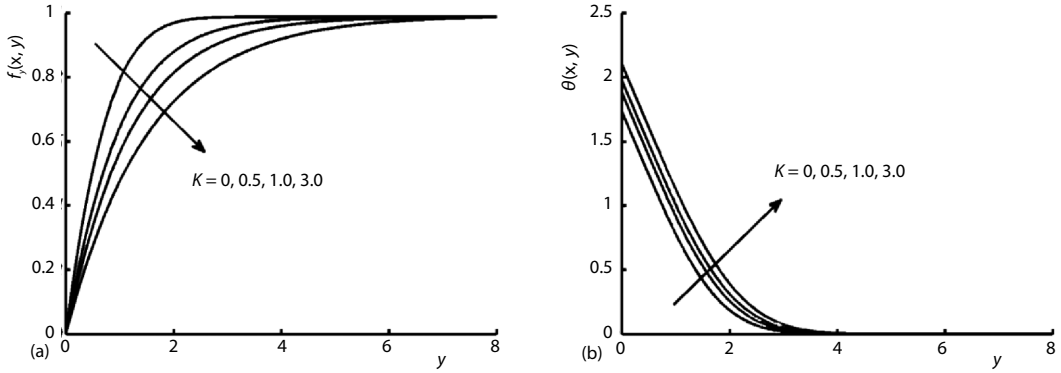


**Figure 11. (a) The variation in velocity and (b) temperature in case of blunt orientation for various values of viscoelastic parameter, $K$, when $\lambda = 2$, $b/a = 0.5$, and Pr = 1**

## Conclusions

In the present theoretical study, we investigated the mixed convection boundary-layer flow of a viscoelastic fluid over the surface of a horizontal cylinder of elliptic cross-section subjected to a constant surface heat flux. The boundary-layer equations governing the flow and heat transfer are transformed to non-dimensional, non-linear system of PDE which is solved by an efficient finite difference scheme (Keller-box method). The effects of viscoelasticity, mixed convection parameter, aspect ratio parameter and the Prandtl number over the flow and heat transfer rates are carefully observed. The present study provides a useful data for devising a most efficient cooling system. It leads to the following inferences.

- By increasing the value of mixed convection parameter, both flow and heat transfer rates enhanced for both the orientations.

- In cooled cylinder case, flow and heat transfer rates reduces in blunt orientation by increasing the aspect ratio but in slender orientation both flow and heat transfer rates increase for $0 < b/a < 0.5$ and decrease fo $0.5 < b/\mathrm{a} < 1$.
- In heated cylinder case, the flow rate increases in both blunt and cylinder orientations with increase in the aspect ratio whereas heat transfer rate increases in slender orientation by the rise in aspect ratio. On the other hand, in blunt orientation it increases along the surface of cylinder in range $0 < \alpha < 42^{\circ}$ changes its behavior in $42^{\circ} < \alpha < 69^{\circ}$ and then decreases in $69^{\circ} < \alpha < 86^{\circ}$.
- Both flow and heat transfer rates decrease in the both orientation cases by enhancing the viscoelasticity of the fluid.
- The rise in Prandtl number results in reduction of both the flow and heat transfer rates in the blunt orientations and exhibit opposite behavior in the slender orientation, and
- The velocity of the fluid in the boundary-layer decreases but temperature rises by enhancing viscoelasticity of the fluid.

## Nomenclature

$a$, $b$ – length of semi major and minor axes, [m]
$C_f$ – skin friction coefficient, [–]
$C_p$ – specific heat constant, [$m^2s^{-2}K^{-1}$]
$f$ – dimensionless stream function, [–]
Gr – Greshof number, [–]
g – acceleration due to gravity, [$ms^{-2}$]
$K$ – non-dimensional viscoelastic parameter, [–]
$k$ – thermal conductivity, [$kgms^{-3}K^{-1}$]
$k_0$ – viscoelastic material parameter, [$kgm^{-1}$]
Nu – Nusselt number, [–]
Pr – Prandtl number, [–]
$q_w$ – wall heat flux, [$kgs^{-3}$]
Re – Reynolds number, [–]
$T$ – temperature of the fluid in the boundary-layer, [K]
$T_\infty$ – ambient fluid temperature, [K]
$U_\infty$ – free steam velocity, [K]
$\overline{u}$, $\overline{v}$ – velocity components in $\overline{x}$- and $\overline{y}$-directions, respectively, [–]
$\overline{u}_e$ – free stream velocity
$\overline{x}$, $\overline{y}$ – dimensional co-ordinates along and normal to the surface of cylinder, respectively, [m]
$x$, $y$ – dimensionless co-ordinates along and normal to the surface of cylinder, respectively, [m]

*Greek symbols*

$\alpha$ – eccentric angle, [–]
$\beta$ – thermal expansion coefficient, [$K^{-1}$]
$\theta$ – dimensionless temperature, [–]
$\lambda$ – mixed convection parameter, [–]
$\mu$ – dynamic viscosity
$\nu$ – kinemic viscosity, [$m^2s^{-1}$]
$\rho$ – fluid density, [$kgm^3$]
$\tau_w$ – surface shear stress, [$kgm^{-1}s^{-2}$]
$\phi$ – angle measured between downward vertical and outer perpendicular, [°]
$\psi$ – dimensionless stream function, [–]

*Superscript*

' – differentiation with respect to $y$

*Subscripts*

w – condition at the surface
$\infty$ – condition far away from the surface

*Acronyms*

PHF – prescribed surface heat flux
PST – prescribed surface temperature

## References

[1] Merkin, J. H., Free Convection Boundary Layers on Cylinders of Elliptic Cross Section, *J. Heat Transfer*, *99* (1977), 3, pp. 453-457
[2] Merkin, J. H., Mixed Convection from a Horizontal Circular Cylinder, *Int. J. Heat Mass Transfer*, *20* (1977), 1, pp. 73-77
[3] Bhatacharyya, S., Pop, I., Free Convection from Cylinder of Elliptic Cross Section in Micropolar Fluids, *Int. J. Eng. Sci.*, *34* (1996), 11, pp. 1301-1310
[4] Hossain, M. A., *et al*., Effect of Thermal Radiation on Natural Convection over Cylinders of Elliptic Cross Section, *Acta Mech.*, *42* (1998), 3-4, pp. 177-186
[5] Ahmad, S., *et al*., Free Convection Boundary Layer Flow over Cylinders of Elliptic Cross Section with Constant Surface Heat Flux, *Eur. J. Sci. Res.*, *23* (2008), 4, pp. 613-625

[6] Javed, T., *et al*., Effect of Thermal Radiation on Unsteady Mixed Convection Flow Near Forward Stagnation Point over a Cylinder of Elliptic Cross Section, *Thermal Science*, *21* (2017), 1, pp. 243-254
[7] Javed, T., *et al*., Mixed Convection Boundary Layer Flow over a Horizontal Elliptic Cylinder with Constant Heat Flux, *Z. Angew. Math. Phys.*, *66* (2015), 6, pp. 3393-3403
[8] Rashidi, M. M., *et al*., Mixed Convective Heat Transfer for MHD Viscoelastic Fluid Flow over a Porous Wedge with Thermal Radiation, *Advances in Mechanical Engineering*, *6* (2014), Jan., ID 735939
[9] Garoosi F., *et al*., Two-Phase Mixture Modeling of Mixed Convection of Nanofluids in a Square Cavity with Internal and External Heating, *Powder Technology*, *275* (2015), May, pp. 304-321
[10] Beg, O. A., *et al*., Double-Diffusive Radiative Magnetic Mixed Convective Slip Flow with Biot and Richardson Number Effects, *Journal of Engineering Thermophysics*, *23* (2014), 2, pp. 79-97
[11] Rashidi, M. M., *et al*. Group Theory and Differential Transform Analysis of Mixed Convective Heat and Mass Transfer from a Horizontal Surface with Chemical Reaction Effects, *Chemical Engineering Communications, 199* (2012), 8, pp. 1012-1043
[12] Dunn, J. E., Rajagopal, K. R., Fluids of Differential Type: Critical Review and Thermodynamic Analysis, *Int. J. Eng. Sci.*, *33* (1995), 5, pp. 689-729
[13] Ariel, P. D., Stagnation Point Flow of a Viscoelastic Fluid Towards a Moving Plate, *Int. J. Eng. Sci.*, *33* (1995), 11, pp. 1679-1687
[14] Rajagopal, K. R., *et al*., Flow of Viscoelastic Fluids between Plates Rotating about Distinct Axes, *Rheol. Acta*, *25* (1986), 5, pp. 459-467
[15] Cortell, R. A., Note on Flow and Heat Transfer of a Viscoelastic Fluid over a Stretching Sheet, *Int. J. Non-Linear Mech.*, *41* (2006), 1, pp. 78-85
[16] Abel, M. S., *et al*., Study of Visco-Elastic Fluid Flow and Heat Transfer over a Stretching Sheet with Variable Viscosity, *Int. J. Non-Linear Mech.*, *37* (2002), 1, pp. 81-88
[17] Hayat, T., *et al*., Mixed Convection Flow of a Micropolar Fluid over a Non-Linear Stretching Sheet, *Physics Letters A*, *372* (2008), 5, pp. 637-647
[18] Sajid, M., *et al*., Boundary Layer Flow of an Oldroyed B Fluid in the Region of Stagnation Point over a Stretching Sheet, *Canadian J. of Physics*, *88* (2010), Sept., pp. 635-640
[19] Abbas, Z., *et al*., Mass Transfer in Two MHD Viscoelastic Fluids over a Shrinking Sheet in Porous Medium with Chemical Reaction Species, *J. Porous Media*, *16* (2013), 7, pp. 619-636
[20] Abbas, Z., *et al*., Hydromagnetic Stagnation Point Flow of a Micropolar Viscoelastic Fluid Towards a Stretching/Shrinking Sheet in the Presence of Heat Generation, *Can. J. Phys.*, *92* (2014), 10, pp. 1113-1123
[21] Abbas, Z., *et al*., Chemically Reactive Hydromagnetic Flow of a Second Grade Fluid in a Semi-Porous Channel, *J. Appl. Mech. Tech. Phys.*, *56* (2015), 5, pp. 878-888
[22] Anwar, I. *et al*., Mixed Convection Boundary Layer Flow of a Viscoelastic Fluid over a Horizontal Circular Cylinder, *Int. J. Non-Linear Mech., 43* (2008), 9, pp. 814-821
[23] Kasim, A. R. M., *et al*., Constant Heat Flux Solution for Mixed Convection Boundary Layer Viscoelastic Fluid, *Heat Mass Transfer, 49* (2013), 2, pp. 163-171
[24] Ahmad, H., *et al*., Radiation Effect on Mixed Convection Boundary Layer Flow of a Viscoelastic Fluid over a Horizontal Circular Cylinder with Constant Heat Flux, *Journal of Applied Fluid Mechanics*, *9* (2016), 3, pp. 1167-1174
[25] Garg, V. K., Rajagopal, K. R., Stagnation Point Flow of a Non-Newtonian Fluid, *Mech. Res. Commun.*, *17* (1990), 6, pp. 415-421
[26] Keller, H. B., Cebeci, T., Numerical Methods in Boundary Layer Theory, *Annual Rev. Fluid Mech.*, *Vol. 10* (1978), Jan., pp. 417-33
[27] Cebeci, T., Bradshaw, P., *Physical and Computational Aspects of Convective Heat Transfer,* Springer, New York, USA, 1984
[28] Nazar, R., *et al*., Mixed Convection Boundary Layer Flow from a Horizontal Circular Cylinder with a Constant Surface Heat Flux, *Int. J. Heat Mass Transfer*, *40* (2004), 3-4, pp. 219-227

Paper submitted: January 20, 2015
Paper revised: December 8, 2016
Paper accepted: December 11, 2016